Engineering Molecular Models: Efficient Parameterization Procedure and Cyclohexanol as Case Study

Thorsten Merker [*], Jadran Vrabec[†], and Hans Hasse[*] [‡]

[*] *Laboratory of Engineering Thermodynamics, University of Kaiserslautern, 67633 Kaiserslautern, Germany*

[†] *Thermodynamics and Energy Technology, University of Paderborn, 33098 Paderborn, Germany*

Abstract

Molecular models for applications in engineering are parameterized using a strategy based on quantum mechanical (QM) ab initio *calculations and thermodynamic data. A new procedure for adjusting such molecular models to thermodynamic data via reduced units is introduced. As a case study, it is applied for developing a new molecular model of cyclohexanol. Compared to experimental data, the resulting molecular model for cyclohexanol shows mean unsigned errors of 0.2 % in saturated liquid density and 3 % in vapor pressure over the whole temperature range from triple point to critical point. The model is used to predict the second virial coefficient and the transport properties, the average deviations from experimental data are 0.1 l/mol and 25 %, respectively.*

Keywords: molecular modeling, parameterization strategy, cyclohexanol, vapor-liquid equilibrium, transport properties

Introduction

Molecular modeling and simulation is a promising approach for describing and predicting thermophysical properties of both pure substances and mixtures for engineering applications (1, 2). Unfortunately, the more widespread use of molecular methods in engineering applications is still restricted by the poor availability of suitable molecular models, which yield the desired properties with the necessary accuracies at moderate simulation effort.

For developing such models, efficient parameterization strategies are necessary. Within DFG's (3) Priority Program 1155 "Molecular Modeling and Simulation

[‡]Author to whom correspondence should be adressed: Tel.: +49-631/205-3497, Fax: +49-631/205-3835, Email: hans.hasse@mv.uni-kl.de

for Process Engineering", an efficient parameterization strategy, using quantum mechanical (QM) *ab initio* calculations and thermodynamic data was developed (4). That strategy was applied for developing rigid, non-polarizable molecular models of comparatively small molecules. The models have state-independent parameters. For computational efficiency, the united-atom approach was used, i.e. hydrogen atoms bound to carbon were not modeled explicitly. The strategy uses information determined by QM *ab initio* calculations to include physically sound molecular properties and to reduce the number of adjustable parameters. A remaining subset of model parameters – typically two to four – is subsequently optimized to experimental data on vapor-liquid equilibria (VLE) of the pure substances. The target is to achieve accuracies in describing experimental data for the vapor pressure, saturated liquid density, and enthalpy of vaporization in the range from triple point to critical point of the order of 5, 1, and 5%, respectively, or below.

In the present paper a new efficient parameter refinement method, using reduced molecular simulation results, is proposed. With this method, the usually difficult last step of the parameterization process can be accelerated. It is exemplified for the case of cyclohexanol. Cyclohexanol is an important intermediate in the industrial production of nylon. A new pair potential for cyclohexanol is introduced here, which is based on seven LJ sites and three point charges.

Overview of Molecular Models for applications in Process Engineering

During the last decade, molecular models for about 95 real fluids were published by our group. Many of them were developed within DFG's Priority Program 1155. First, simple molecular models consisting of one Lennard Jones site (1CLJ) and the two-center Lennard Jones plus point dipole (2CLJD) or point quadrupole (2CLJQ) pair potential (5, 6) for describing small molecules like Argon or halogenated hydrocarbons were developed. The modeling approach used for these fluids was based on a systematic study of the VLE of model fluids (7, 8) for developing global correlations in terms of the molecular parameters of the used pair potentials.

Later on, molecular models for hydrogen bonding fluids were developed(9–13). For these substances the models consist of multi-center Lennard Jones (MCLJ) pair potentials plus point charges. The point charges account for both polarity and hydrogen bonding. For this model type, results from QM *ab initio* calculations were used for the geometry parameters as discussed in the Section "Molecular properties from QM".

Recently, using the same approach, a set of MCLJ pair potentials plus point dipole and/or point quadrupole were developed for describing small molecules, like hydrogen cyanide, but also larger cycloalkanes, like cyclohexane(4, 14, 15).
Table 1 gives a summary of these models.

Molecular properties from QM

A detailed description of the QM based parameterization strategy was reported recently by Eckl et al. (4) so that it is only summarized here briefly.
The geometry of the molecular models, i.e. bond lengths, angles, and dihedrals, are directly taken from QM calculations. The geometry optimization, by energy minimization, is carried out using GAMESS(US) (16). The Hartree-Fock level of theory is applied with a relatively small (6-31G) basis set. Alternatively, density functional theory (DFT) methods, e.g. BLY3P, can be used, as they are known to give reasonable results for the molecular structure (17).
For determining the charge distribution of the molecule the Møller-Plesset 2 level is used that takes into account electron correlation in combination with the polarizable 6-311G(d,p) basis set. For the calculation of the electrostatic moments for the development of engineering molecular models, a liquid-like state should rather be considered than the isolated molecule in the ideal gas state. This is done by placing the molecule within a dielectric continuum and assigning the experimental dielectric constant of the liquid to the continuum by the COSMO method (18). From the resulting electron density distribution, point dipoles and point quadrupoles are estimated by simple integration over the orbitals. Magnitudes and orientations of these electrostatic interaction sites are used in the molecular models without any modification. All point dipoles and point quadrupoles are placed at the center of mass (COM).
A similar procedure is used for molecular models with point charges for hydrogen bonding fluids (9). Here, three point charges account for both polarity and hydrogen bonding. E.g., for methanol, one point charge is located at the hydroxyl hydrogen atom position and one at the LJ site of the hydroxyl group. The third point charge is superimposed to the LJ site of the CH3 group, where its magnitude is determined by the overall electroneutrality of the molecule. The geometry parameters are also taken directly from QM calculations but the two free point charge magnitudes are optimized using the same procedure as for the LJ parameters as described below.
Subsequently, the parameters for the dispersive and repulsive interactions are fitted in the optimization process to yield the correct VLE behavior of the modeled pure substance. The optimization is performed using a Newton scheme as proposed by Stoll (19). It relies on a least-square minimization of a weighted fitness

function that quantifies the deviations of simulation results from a given molecular model compared to experimental data.
For the case study cyclohexanol, correlations for vapor pressure, saturated liquid density, and enthalpy of vaporization, taken from the DIPPR database (20), were used as "experimental data" for model adjustment and evaluation. This was done even in cases where the correlation is based on no or only few true experimental data points, as the correlations are regarded best practice. The comparison between simulation results and experiment was done by applying fits to the simulation data according to Lotfi et al. (21). The relative deviation between fit and correlation is calculated in steps of 1 K from 55 to 97% of the critical temperature and is denoted by "mean unsigned error" in the following.
Vapor-liquid equilibrium simulations were performed using the Grand Equilibrium method by Vrabec et al. (22), technical simulation details are given in the Appendix.

Reduced Unit Method for Optimizing Molecular Models

In most molecular simulation programs reduced units are used internally to describe physical properties. The reduced properties, i.e. dimensionless, are labeled with an asterisk here. Typically, energy ε_R, length σ_R and mass m_R are chosen as reference values for the reduction. This applies to all properties that are evaluated during simulation such as temperature $T^* = Tk_\mathrm{B}/\varepsilon_\mathrm{R}$ potential energy $E^* = E/\varepsilon_\mathrm{R}$, intermolecular forces $f^* = f\sigma_\mathrm{R}/\varepsilon_\mathrm{R}$ or torques $\tau^* = \tau/\varepsilon_\mathrm{R}$, where k_B is the Boltzman constant, but also to aggregated thermodynamic data such as pressure $p^* = p\sigma_\mathrm{R}^3/\varepsilon_\mathrm{R}$ or chemical potential $\tilde{\mu}_\mathrm{i}^* = \tilde{\mu}_\mathrm{i}/\varepsilon_\mathrm{R}$, which are usually the goal of a molecular simulation run.
Note that all parameters of the molecular model are also applied in their reduced form, i.e. the positions of the interaction sites are scaled by

$$x_\mathrm{i}^* = x_\mathrm{i}/\sigma_\mathrm{R}, \tag{1}$$

$$y_\mathrm{i}^* = y_\mathrm{i}/\sigma_\mathrm{R}, \tag{2}$$

$$z_\mathrm{i}^* = z_\mathrm{i}/\sigma_\mathrm{R}, \tag{3}$$

the LJ site parameters by

$$\sigma_\mathrm{i}^* = \sigma_\mathrm{i}/\sigma_\mathrm{R}, \tag{4}$$

$$\varepsilon_\mathrm{i}^* = \varepsilon_\mathrm{i}/\varepsilon_\mathrm{R}, \tag{5}$$

as well as the magnitudes of the electrostatic sites, i.e. for the point charge magnitude

$$q_{\mathrm{i}}^{*} = q_{\mathrm{i}} / \sqrt{4\pi\varepsilon_0\sigma_{\mathrm{R}}\varepsilon_{\mathrm{R}}}, \tag{6}$$

the dipole moment

$$\mu_{\mathrm{i}}^{*} = \mu_{\mathrm{i}} / \sqrt{4\pi\varepsilon_0\sigma_{\mathrm{R}}^{3}\varepsilon_{\mathrm{R}}}, \tag{7}$$

and the quadrupole moment

$$Q_{\mathrm{i}}^{*} = Q_{\mathrm{i}} / \sqrt{4\pi\varepsilon_0\sigma_{\mathrm{R}}^{5}\varepsilon_{\mathrm{R}}}, \tag{8}$$

where ε_0 is the permittivity of vacuum. On the basis of a reduced molecular model, the vapor-liquid equilibrium simulations are performed yielding e.g., reduced values for vapor pressure p^*, saturated densities $\rho^{'*}$, $\rho^{''*}$ and enthalpy of vaporization $\Delta h_{\mathrm{v}}^{*}$. For comparison with experimental data, these reduced quantities are converted back to SI units via

$$T = T^{*}\varepsilon_{\mathrm{R}}/k_{\mathrm{B}}, \tag{9}$$

$$p = p^{*}\varepsilon_{\mathrm{R}}/\sigma_{\mathrm{R}}^{3}, \tag{10}$$

$$\rho = \rho^{*}/\sigma_{\mathrm{R}}^{3}, \tag{11}$$

$$\Delta h_{\mathrm{v}} = \Delta h_{\mathrm{v}}^{*}\varepsilon_{\mathrm{R}}, \tag{12}$$

$$D = D^{*}\frac{\sigma_{\mathrm{R}}}{\sqrt{m_{\mathrm{R}}/\varepsilon_{\mathrm{R}}}}, \tag{13}$$

$$\eta = \eta^{*}\frac{\sqrt{m_{\mathrm{R}}\varepsilon_{\mathrm{R}}}}{\sigma_{\mathrm{R}}^{2}}, \tag{14}$$

$$\lambda = \lambda^{*}\frac{k_{\mathrm{B}}}{\sigma_{\mathrm{R}}^{2}\sqrt{m_{\mathrm{R}}/\varepsilon_{\mathrm{R}}}} \tag{15}$$

Where D denotes the self-diffusion coefficient, η the shear viscosity and λ the thermal conductivity.

Central to this approach is that the simulation results are strictly valid for *any* choice of the triple ε_{R}, σ_{R} and m_{R}. Furthermore, it should be noted that the static thermodynamic properties, i.e. non-transport data, do not depend on the mass m_{R}. Therefore, for a given simulation result in reduced units, one may choose ε_{R}, σ_{R} and m_{R} to achieve an optimal agreement with the experimental target data without carrying out new simulations. Thereby, of course a new molecular model is generated. This new model is identical with the one for which the simulation was performed only in reduced units but not in the real properties and parameters in SI units. An optimization based on that idea is especially attractive for an

efficient fine tuning of molecular models which already represent the target data fairly well.

Note that that the pressure and the density in real units depend on the reference size σ_R to the power of three. Thus small variations in σ_R lead to significant changes in these properties that are used for optimization here.

To illustrate this procedure, the dependence of VLE and transport properties of cyclohexanol on the scaling parameters ε_R, σ_R and m_R is studied. The baseline for the variation of ε_R, σ_R and m_R is the optimal cyclohexanol model which is described below.

Both ε_R and σ_R were changed by ± 5 %, while m_R was changed by ± 20 % around the baseline values to study the effect on the different thermophysical properties. The results are shown in Figures 1 to 6. The blue lines correspond to the variation of ε_R, the red lines to variations of σ_R and the green lines to variations of m_R. Note that, given the baseline simulation results, no new simulations are needed to study the variations presented here.

The influence of the variations of ε_R and σ_R on the saturated densities is shown in Figure 1. An increase of ε_R leads to an increase in the saturated densities, whereas an increase of σ_R leads to an decrease of the saturated densities.

Figure 2 shows the influence of ε_R and σ_R on the vapor pressure. An increase of ε_R leads to a decrease of the vapor pressure, the same holds for an increase of σ_R. The sensitivity of the vapor pressure is stronger for ε_R than for σ_R, as ε_R influences both T and p, cf. Equations (9) and (10).

In Figure 3 the influence of variations of ε_R on the enthalpy of vaporization is shown. Variations of σ_R show no influence on the enthalpy of vaporization. An increase of ε_R leads to an increase of the enthalpy of vaporization.

The dependence of the self-diffusion coefficient on variations of ε_R, σ_R and m_R is shown in Figure 4. An increase in ε_R or σ_R leads to an increase in the self-diffusion coefficient, whereas m_R has the opposite effect. ε_R has the strongest influence on the self-diffusion coefficient as it influences both T and D, cf. Equations (9) and (13).

Figure 5 shows the results for the shear viscosity. An increase in ε_R or m_R leads to an increase in the shear viscosity, whereas σ_R has the opposite effect. Again the sensitivity is highest for ε_R due to its influence on both T and η, cf. Equations (9) and (14).

Finally, the dependence of the thermal conductivity on variations of ε_R, σ_R and m_R is shown in Figure 6. An increase in σ_R and m_R leads to an decrease in the thermal conductivity whereas an increase in ε_R leads to an increase in the thermal conductivity. As for the other transport properties, ε_R influences the thermal conductivity the most as it changes both T and λ, cf. Equations (9) and (15).

For the optimization itself any method can be used. Eg. when taking the squared sum of relative deviations to experimental data as objective function

$$\delta = \sum_{i=1}^{n} \left(\frac{z_i^{sim}(\varepsilon_R, \sigma_R) - z_i^{exp}}{z_i^{exp}} \right)^2 \tag{16}$$

new values for the simulated property $z_i^{sim}(\varepsilon_R, \sigma_R)$ can be generated using Equations (9) to (15) from the reduced properties determined in a baseline simulation without any new simulation. Any mathematical scheme can be applied.

Cyclohexanol

Molecular Model

A new cyclohexanol model was developed based on QM calculations and subsequently optimized using experimental vapor pressure, bubble density and enthalpy of vaporization as described above using the reduced unit method. As the complexity of a molecular model determines the computing time during molecular simulation, it was attempted here to find an efficient solution balancing accuracy and simplicity. A rigid model with seven LJ sites and three point charges was chosen. The internal degrees of freedom were neglected, as the cyclohexane ring predominantly assumes in the energetically favorable chair-conformation.
The geometric parameters of the molecular model were taken directly from QM calculations, as described in the Section "Molecular properties from QM". One LJ site was located exactly at all resulting nuclei positions, except for the hydrogen atom. The methylene CH_2 and methine CH group were modeled by a single LJ site, i.e. the united-atom approach was used. The coordinates of the seven LJ sites are given in Table 2 and a graphic schematic is presented in Figure 7.
A subset of the parameters for the LJ sites and the point charges was optimized to the DIPPR correlations for saturated liquid density and vapor pressure of pure cyclohexanol (20) in the range from 390 to 620 K. As a starting point for optimization, the LJ parameters for the methylene CH_2 site were taken from a cyclohexane model by Eckl et al. (4). The remaining LJ parameters for the methine CH and hydroxyl OH group and the point charges were taken from Schnabel et al. (11). During the optimization, only the LJ parameters of the methylene CH_2 sites and the point charges were adjusted. The method of Stoll (19) was used for the first step of this optimization. The result of this step is shown in Figures 8 to 10. In a second step, the reduced unit method was used for a subsequent optimization. The final model was generated by changing ε_R by $+1.6$ %. The result is also shown in Figures 8 to 10. To verify the results of the reduced unit method, which were obtained without further simulations after step one, cf. Table 3, an additional set of VLE simulations, cf. Table 4, was carried out for the final model as shown in

Figures 8 to 11, which is in very good agreement with the result from the reduced unit method as expected.

Vapor-liquid equilibria

VLE of the new cyclohexanol model are presented together with a DIPPR correlation (20) in Figures 8 to 11 and in Tables 4 and 3. The agreement between the molecular model and the experimental data is very good. The mean unsigned errors in vapor pressure, saturated liquid density and enthalpy of vaporization are 3, 0.2, and 12 %, respectively, in the temperature range from 390 to 620 K, which is about 50 to 97 % of the critical temperature. The correspond numbers for the deviations found for the initial model after step one were 19, 1.7 and 9 %, respectively. The seemingly high mean unsigned error for the enthalpy of vaporization is mainly due to the lack of experimental data for cyclohexanol. In fact, experimental data (23) are only available for the enthalpy of vaporization at about 420 K where the present molecular model shows a good agreement, cf. Figure 10. The DIPPR correlation for the enthalpy of vaporization as shown in Figure 10 is unusually "flat" near the critical point. Using that correlation for predicting the gas phase density near the critical point via the Clausius-Clapeyron relation, results in an unusual asymmetric shape of the saturated density plot as shown in Figure 8. We conclude that the DIPPR correlation for the enthalpy of vaporization of cyclohexanol is wrong.

Second Virial Coefficient

The predicted second virial coefficient is compared to a DIPPR correlation (20) in Figure 12. It was calculated by evaluating Mayer's f-function as reported by Eckl et al. (15) The present model overestimates the second virial coefficient only by about 0.1 l/mol throughout the entire regarded temperature range from 325 to 1500 K which is within the uncertainty of the correlation.

Transport properties

Transport properties of cyclohexanol were obtained by equilibrium molecular dynamics (EMD) simulations following the Green-Kubo formalism. This approach is based on the relationship between the transport coefficients and the time integrals of corresponding autocorrelation functions of microscopic fluxes in a system in equilibrium. The calculation details are similar to those recently reported by Guevera at al. (24) and are not repeated here. Technical simulation details are given in the Appendix. Numerical results are presented in Table 13

In Figure 13, the predicted self-diffusion coefficient is compared to a correlation of experimental data by O' Reilly et al. (25) The present predictions are above the data by O' Reilly et al. (25) for temperatures below 400 K. For higher temperatures, the predictions are below the experimental data with a mean deviation of 20 %.
The predictions for the shear viscosity are compared to experimental data by Friend and Hargreaves (26) and to a DIPPR correlation (20) in Figure 14. Here, the predictions underestimate the experiment (20, 26) over the whole temperature range with a mean deviation of 25 %.
The thermal conductivity was also predicted by EMD simulation. In Figure 15, these data are compared to the experimental data (27) and a DIPPR correlation (20). The high statistical simulation uncertainties are due to the strongly interacting molecules, causing long time behaviors of the thermal conductivity autocorrelation function. As EMD is not well suited for determining the thermal conductivity, non-equilibrium molecular dynamics simulations (28) (NEMD) at these state points should yield statistically more sound data. Nevertheless, a sufficient accuracy for a first assessment was achieved. The predictions for the thermal conductivity are above the experimental data (27)for temperatures higher than 380 K. The mean deviation is around 30 % but the simulation data agree with the experimental data almost throughout within their large statistical uncertainties.

Conclusion

An overview is given on the 95 molecular models for application in process engineering and their development published by our group. Starting from simple 1CLJ pair potentials also more complex polar MCLJ models were parameterized. With rising complexity of the molecular models, new modeling approaches were developed as well. Recently, Eckl et al. proposed a new strategy using results from QM *ab initio* calculations to include physically sound molecular properties and to reduce the number of adjustable parameters. The remaining parameters were adjusted to experimental VLE data, i.e. saturated liquid density, vapor pressure and enthalpy of vaporization.
In this work, a new optimization strategy is proposed for the refined adjustment of the remaining parameters. Reduced molecular simulation results can be adjusted to experimental data by variation of the reference values ε_R, σ_R and m_R used in simulation codes to define dimensionless variables. This optimization can be carried out without any new molecular simulations runs and is attractive for the time consuming fine tuning of molecular models. The sensitivity of various thermophysical properties regarding variations of ε_R, σ_R and m_R is studied for the case of cyclohexanol.

A pair potential for cyclohexanol was developed with the new method. The model consists of seven LJ sites and three point charges. The parameters of the model were adjusted with the modeling approach by Eckl et al., the optimization following Stoll and with the reduced unit strategy proposed here. The final model shows mean unsigned errors of 0.2 % in saturated liquid density and 3 % in vapor pressure over the whole temperature range from triple point to 97 % of the critical point.
The second virial coefficient was predicted with an insignificant offset to a DIPPR correlation. EMD simulations were preformed to predict transport properties. The predictions for the self-diffusion coefficient, the shear viscosity and the thermal conductivity shows relative deviations of around 25 % compared to experimental data, which is satisfying as they were not considered in the parameterization.

Acknowledgment

The authors gratefully acknowledge financial support by Deutsche Forschungsgemeinschaft, Priority Program 1155 "Molecular Modeling and Simulation in Process Engineering". The presented research was conducted under the auspices of the Boltzmann-Zuse Society of Computational Molecular Engineering (BZS). The simulations were performed on the national super computer NEC SX-8 at the High Performance Computing Centre Stuttgart (HLRS) under the grant MMHBF and on the HP XC4000 supercomputer at the Steinbruch Centre for Computing under the grant LAMO.

Simulation Details

In this work, the Grand Equilibrium method (22) was used for VLE calculations. To determine the chemical potential in the liquid, gradual insertion (29) was used. For gradual insertion, Monte Carlo simulations in the NpT ensemble were performed using 500 molecules. Starting from a face centered cubic lattice, 15 000 Monte Carlo cycles were sampled for equilibration with the first 5 000 time steps in the canonical (NVT) ensemble and 100 000 for production, each cycle containing 500 displacement moves, 500 rotation moves, and 1 volume move. Every 50 cycles, 5 000 fluctuating state change moves, 5 000 fluctuating particle translation/rotation moves and 25 000 biased particle translation/rotation moves were performed, to determine the chemical potential.
For the corresponding vapor, Monte Carlo simulations in the pseudo-μVT ensemble were carried out. The simulation volume was adjusted to lead to an average number of 500 molecules in the vapor phase. After 10 000 initial NVT Monte

Carlo cycles, starting from a face centered cubic lattice, 25 000 equilibration cycles in the pseudo-μVT ensemble were performed. The length of the production run was 100 000 cycles. One cycle is defined here to be a number of attempts to displace and rotate molecules equal to the actual number of molecules plus two insertion and two deletion attempts.
The cut-off radius was set to at least 18 Å and a center of mass cut-off scheme was employed. Lennard-Jones long-range interactions beyond the cut-off radius were corrected as proposed by Lustig (30). Statistical uncertainties in the simulated values were estimated by a block averaging method (31).
The second virial coefficient was calculated by evaluating Mayer's f-function at 563 radii from 2 to 24 Å, averaging over 1000^2 random orientations at each radius. The random orientations were generated using a modified Monte Carlo scheme (4, 32). A cut-off correction was applied for distances larger than 24 Å for the LJ potential (30). The electrostatic interactions need no long-range correction as they vanish by angle averaging.
EMD simulations for transport properties were made in two steps. In the first step, a short simulation in the isobaric-isothermal (NpT) ensemble was performed at the specified temperature and pressure to calculate the respective density. In the second step, a canonic (NVT) ensemble simulation was made at this temperature and density, to determine the transport properties. The simulations were carried out in a cubic box with periodic boundary conditions containing at least 2048 molecules. In all EMD simulations, the integration time step was 1 fs. The cut-off radius was set to 18 Å. The simulations were equilibrated in the NVT ensemble over 10 000 time steps, followed by production runs of 1 000 000 time steps. The sampling length of the autocorrelation functions was between 11 and 26 ps.

References

[1] P. Ungerer, C. Nieto-Draghi, B. Rousseau, G. Ahunbay, and V. Lachet. *J. Mol. Liq.*, 134:71–89, 2007.

[2] P. Ungerer, C. Nieto-Draghi, V. Lachet, A. Wender, A. Di Lella, A. Boutin, B. Rousseau, and A.H. Fuchs. *Mol. Sim.*, 33:15–30, 2007.

[3] Deutsche forschungsgemeinschaft (german research foundation). http://www.dfg.de.

[4] B. Eckl, J. Vrabec, and H. Hasse. *J. Phys. Chem. B*, 112:12710–12721, 2008.

[5] J. Vrabec, J. Stoll, and H. Hasse. *J. Phys. Chem. B*, 105:12126–12133, 2001.

[6] J. Stoll, J. Vrabec, and H. Hasse. *J. Chem. Phys.*, 119:11396–11407, 2003.

[7] J. Stoll, J. Vrabec, H. Hasse, and J. Fischer. *Fluid Phase Equilib.*, 179:339–362, 201.

[8] J. Stoll, J. Vrabec, H. Hasse, and J. Fischer. *Fluid Phase Equilib.*, 209:29–53, 2003.

[9] T. Schnabel, J. Vrabec, and H. Hasse. *Fluid Phase Equilib.*, 233:134–143, 2005.

[10] T. Schnabel, J. Vrabec, and H. Hasse. *Fluid Phase Equilib.*, 239:125–126, 2006.

[11] T. Schnabel, M. Cortada, J. Vrabec, S. Lago, and H. Hasse. *Chem. Phys. Lett.*, 435:268–272, 2007.

[12] T. Schnabel, A. Srivastava, J. Vrabec, and H. Hasse. *J. Phys. Chem. B*, 111:9871–9878, 2007.

[13] T. Schnabel, J. Vrabec, and H. Hasse. *Fluid Phase Equilib.*, 263:144–159, 2008.

[14] B. Eckl, J. Vrabec, and H. Hasse. *Fluid Phase Equilib.*, 274:16–26, 2008.

[15] B. Eckl, J. Vrabec, and H. Hasse. *Mol. Phys.*, 106:1039–1046, 2008.

[16] M.W. Schmidt, K.K. Baldridge, J.A. Boatz, S.T. Elbert, M.S. Gordon, J.H. Jensen, S. Koseki, N. Matsunaga, K.A. Nguyen, and Kiet. *J. Comput. Chem.*, 14:1347–1363, 1993.

[17] A. R. Leach. *Molecular Modeling. Principles and Application*. Prentice Hall, Englewood Cliffs, 2001.

[18] A. Klamt. *J. Phys. Chem.*, 99:2224–2235, 1995.

[19] J. Stoll. *Molecular Models for the Prediction of Thermophysical Properties of Pure Fluids and Mixtures*. Reihe 3. VDI-Verlag, Düsseldorf, 2005.

[20] Dippr project 801 - full version. design institute for physical property data/aiche.

[21] A. Lotfi, J. Vrabec, and J. Fischer. *Mol. Phys.*, 76:1319–1333, 1992.

[22] J. Vrabec and H. Hasse. *Mol. Phys.*, 100:3375–3383, 2002.

[23] J. B. Pedley. *Sussex-N.P.L. Computer Analysed Thermochemical Data. Organic and Organometallic Compounds*. University of Sussex, Brighton, England, 1977.

[24] G Guevara-Carrión, C. Nieto-Draghi, J. Vrabec, and H. Hasse. *J. Phys. Chem. B*, 116:16664–16674, 2008.

[25] D. E. O'Reilly, E. M. Peterson, and D. L. Hogenboom. *J. Chem. Phys.*, 57:3969–3976, 1972.

[26] J. N. Friend and W. D. Hargreaves. *Phil. Mag.*, 35:57–64, 1944.

[27] *Thermal Conductivity of Liquid Cycloaliphatic Compounds*. Item 77010, Engineering Science Data, London, 1977.

[28] F. Müller-Plathe. *J. Chem. Phys*, 106:6082, 1997.

[29] J. Vrabec, M. Kettler, and H. Hasse. *Chem. Phys. Lett.*, 356:431, 2002.

[30] M. P. Allen and D. J. Tildesley. *Computer simulations of liquids*. Clarendon Press, Oxford, 1987.

[31] H. Flyvbjerg and H. G. Petersen. *J. Chem. Phys.*, 91:461, 1989.

[32] R. D. Mountain. *J. Phys. Chem. B*, 109:13352, 2005.

Table 1: Overview of molecular models for applications in process engineering published by the author's group. The model parameters can be found in References (4–6, 9–15).

Fluid	CAS RN	Fluid	CAS RN
Non-polar, 1CLJ		**Dipolar, 2CLJD**	
Ne	7440-01-9	R1141 ($CHF{=}CH_2$)	75-02-5
Ar	7440-37-1	$CHBr_2{=}CH_3$	557-91-5
Kr	7439-90-9	$CFBr{=}CF_2$	598-73-2
Xe	7440-63-3	**Quadrupolar, 2CLJQ**	
CH_4	74-82-8	N_2	7727-37-9
Dipolar, 1CLJD		O_2	7782-44-7
R30 (CH_2Cl_2)	75-09-2	Cl_2	7782-50-5
R30B2 (CH_2Br2)	74-95-3	Br_2	7726-95-6
R32 (CH_2F_2)	75-10-5	F_2	7782-41-4
CH_2I_2	75-11-6	I_2	7553-56-2
Dipolar, 2CLJD		CO_2	124-38-9
CO	630-08-0	CS_2	75-15-0
CH_3I	74-88-4	C_2H_2	74-86-2
R10B1 ($CBrCl_3$)	75-62-7	C_2H_4	74-85-1
R11 ($CFCl_3$)	75-69-4	C_2H_6	74-84-0
R12 (CF_2Cl_2)	75-71-8	Propadiene ($CH_2{=}C{=}CH_2$)	463-49-0
R12B1 ($CBrClF_2$)	353-59-3	Propyne ($CH_3{-}C{\equiv}CH$)	74-99-7
R12B2 (CBr_2F_2)	75-61-6	Propylene ($CH_3{-}CH{=}CH_2$)	115-07-1
R13 (CF_3Cl)	75-72-9	SF_6	2551-62-4
R13B1 ($CBrF_3$)	75-63-8	R10 (CCl_4)	56-23-5
R20 ($CHCl_3$)	67-66-3	R14 (CF_4)	75-73-0
R20B3 ($CHBr_3$)	75-25-2	R113 ($CFCl_2{-}CF_2Cl$)	76-13-1
R21 ($CHFCl_2$)	75-43-4	R114 ($CF_2Cl{-}CF_2Cl$)	76-14-2
R22 (CHF_2Cl)	75-45-6	R114B2 ($CBrF_2{-}CBrF_2$)	124-73-2
R23 (CHF_3)	75-46-7	R115 ($CF_3{-}CF_2Cl$)	76-15-3
R30B1 (CH_2BrCl)	74-97-5	R134 ($CHF_2{-}CHF_2$)	359-35-3
R40 (CH_3Cl)	74-87-3	R150B2 ($CH_2Br{-}CH_2Br$)	106-93-4
R40B1 (CH_3Br)	74-87-3	R1110 (C_2Cl_4)	127-18-4
R41 (CH_3F)	593-53-3	R1114 (C_2F_4)	116-14-3
R112a ($CCl_3{-}CF_2Cl$)	76-11-9	R1120 ($CHCl{=}CCl_2$)	79-01-6
R123 ($CHCl_2{-}CF_3$)	306-83-2	**Polar, Multi-CLJ**	
R123B1 ($CHClBr{-}CF_3$)	151-67-7	Iso-butane (C_4H_{10})	75-28-5
R124 ($CHFCl{-}CF_3$)	2837-89-0	Cyclohexane (C_6H_{12})	110-82-7
R125 ($CHF_2{-}CF_3$)	354-33-6	Methanol (CH_3OH)	67-56-1
R130a ($CH_2Cl{-}CCl_3$)	630-20-6	Ethanol (C_2H_5OH)	64-17-5
R131b ($CH_2F{-}CCl_3$)	2366-36-1	Formaldehyde ($CH_2 = O$)	50-00-0
R134a ($CH_2F{-}CF_3$)	811-97-2	Dimethylether ($CH_3{-}O{-}CH_3$)	115-10-6
R140 ($CHCl_2{-}CH_2Cl$)	79-00-5	Ammonia (NH_3)	7664-41-7
R140a ($CCl_3{-}CH_3$)	71-55-6	Monomethylamine ($NH_2{-}CH_3$)	74-89-5
R141b ($CH_3{-}CFCl_2$)	1717-00-6	Dimethylamine ($CH_3{-}NH{-}CH_3$)	124-40-3
R142b ($CH_3{-}CF_2Cl$)	75-68-3	R227ea ($CF_3{-}CHF{-}CF_3$)	431-89-0
R143a ($CH_3{-}CF_3$)	420-46-2	Sulfur Oxide (SO_2)	7446-09-5
R150a ($CHCl_2{-}CH_3$)	75-34-3	Ethylene Oxide (C_2H_4O)	75-21-8
R152a ($CH_3{-}CHF_2$)	75-37-6	Dimethylsulfide ($CH_3{-}S{-}CH_3$)	75-18-3
R160B1 ($CH_2Br{-}CH_3$)	74-96-4	Hydrogen Cyanide (NCH)	74-90-8
R161 ($CH_2F{-}CH_3$)	353-36-6	Acetonitrile (NC_2H_3)	75-05-8
R1113 ($CFCl{=}CF_2$)	2366-36-1	Thiophene (SC_4H_4)	110-02-1
R1132 ($CHCl{=}CF_2$)	359-10-4	Formic Acid (CH_2O_2)	64-18-6
R1132a ($CF_2{=}CH_2$)	75-38-7	Nitromethane (NO_2CH_3)	75-52-5
R1140 ($CHCl{=}CH_2$)	75-01-4		

Table 2: Coordinates and parameters of the LJ sites and the point charges in the principal axes system of the new molecular model for cyclohexanol. Bold characters indicate the represented atoms.

Interaction Site	x Å	y Å	z Å	σ Å	ε/k_B K	q e
CH$_2$(1)	-2.21180	-0.54464	0	3.412	104.03	—
CH$_2$(2)	-1.35799	0.46139	-1.57594	3.412	104.03	—
CH$_2$(3)	0.52527	-0.37854	-1.56168	3.412	104.03	—
CH$_2$(4)	0.52527	-0.37854	1.56168	3.412	104.03	—
CH$_2$(5)	-1.01956	0.36185	1.57594	3.412	104.03	—
CH	1.06798	0.36185	0	3.234	61.01	0.278022
OH	2.41338	0.03535	0	3.150	86.50	-0.644173
H-O	2.46899	-0.93682	0	—	—	0.366151

Table 3: Vapor-liquid equilibria of cyclohexanol: results of the reduced unit method (sim) are compared to DIPPR correlation (20) for vapor pressure and saturated liquid densities. The number in parentheses indicates the statistical uncertainty in the last digit.

T	p_{sim}	p_{DIPPR}	ρ'_{sim}	ρ'_{DIPPR}	ρ''_{sim}	$\Delta h^{\mathrm{v}}_{\mathrm{sim}}$
K	MPa	MPa	mol/l	mol/l	mol/l	kJ/mol
396.6	0.033(2)	0.028	8.566(3)	8.557	0.0103(5)	47.06(1)
427.1	0.087(3)	0.082	8.263(3)	8.257	0.0253(8)	43.99(1)
457.7	0.189(4)	0.196	7.914(4)	7.925	0.052 (1)	40.84(1)
488.2	0.393(6)	0.394	7.578(4)	7.583	0.106 (2)	37.76(1)
508.5	0.580(7)	0.588	7.321(5)	7.338	0.155 (2)	35.59(2)
528.8	0.855(9)	0.857	7.071(6)	7.062	0.228 (2)	32.33(2)
559.4	1.36 (1)	1.376	6.622(9)	6.624	0.369 (3)	29.61(2)
589.9	2.12 (2)	2.108	6.11 (2)	6.0864	0.602 (4)	25.28(4)
610.2	2.81 (2)	2.706	5.68 (6)	5.656	0.854 (6)	21.49(5)

Table 4: Vapor-liquid equilibria of cyclohexanol: simulation results (sim) are compared to DIPPR correlation (20) for vapor pressure and saturated liquid densities. The number in parentheses indicates the statistical uncertainty in the last digit.

T	p_{sim}	p_{DIPPR}	ρ'_{sim}	ρ'_{DIPPR}	ρ''_{sim}	$\Delta h^{\mathrm{v}}_{\mathrm{sim}}$
K	MPa	MPa	mol/l	mol/l	mol/l	kJ/mol
390	0.024(2)	0.022	8.632(3)	8.625	0.0075(5)	47.73(2)
420	0.067(2)	0.065	8.335(4)	8.328	0.0197(7)	44.75(2)
450	0.159(4)	0.159	8.007(5)	8.014	0.045 (1)	41.64(2)
480	0.317(6)	0.331	7.660(5)	7.677	0.086 (2)	38.57(2)
500	0.489(7)	0.504	7.431(5)	7.439	0.131 (2)	36.52(2)
520	0.703(9)	0.733	7.180(5)	7.183	0.187 (2)	34.38(2)
550	1.19 (1)	1.202	6.783(6)	6.762	0.321 (3)	30.86(2)
580	1.83 (2)	1.848	6.28 (1)	6.273	0.507 (5)	26.81(3)
600	2.39 (2)	2.394	5.89 (2)	5.883	0.693 (5)	23.62(4)
620	3.14 (2)	3.046	5.45 (6)	5.396	0.986 (7)	19.66(7)

Table 5: Second virial coefficient of cyclohexanol: simulation results (sim) are compared to a DIPPR correlation (20). The numbers in parentheses indicates the statistical uncertainty in the last digits.

T	B_{sim}	B_{DIPPR}
K	mol/l	mol/l
325	-3.1331	-3.6 (9)
350	-2.2748	-2.7 (7)
390	-1.5336	-1.8 (5)
420	-1.2118	-1.4 (4)
450	-0.9898	-1.2 (3)
480	-0.8277	-1.0 (2)
500	-0.7419	-0.9 (2)
520	-0.6691	-0.8 (2)
550	-0.5784	-0.7 (2)
580	-0.5046	-0.6 (1)
600	-0.4624	-0.5 (1)
650	-0.3757	-0.4 (1)
700	-0.3083	-0.37 (9)
800	-0.2103	-0.26 (6)
900	-0.1425	-0.18 (4)
1000	-0.0927	-0.13 (3)
1100	-0.0547	-0.09 (2)
1200	-0.0247	-0.05 (1)
1300	-0.0053	-0.028(7)
1400	0.0194	-0.007(2)
1500	0.0361	0.011(3)

Table 6: Transport properties of cyclohexanol: simulation results (sim) are compared to a correlation of experimental data (25) and DIPPR correlations (20). The numbers in parentheses indicates the statistical uncertainty in the last digits.

T	D_{sim}	D_{exp}	ν_{sim}	ν_{DIPPR}	λ_{sim}	λ_{DIPPR}
K	$10^{-9}\mathrm{m}^2/\mathrm{s}$	$10^{-9}\mathrm{m}^2/\mathrm{s}$	$10^{-3}\mathrm{Pas}$	$10^{-3}\mathrm{Pas}$	$10^{-2}\mathrm{W/mK}$	$10^{-2}\mathrm{W/mK}$
360	0.88(2)	0.6(3)	18(4)	30.50	58(77)	126
380	1.36(1)	1.1(4)	11(2)	17.33	106(32)	124
400	1.95(1)	1.9(5)	9(1)	10.87	147(28)	121
420	2.48(1)	3.0(6)	6(1)	7.31	182(31)	119
440	3.52(1)	4.7(6)	4(1)	5.16	132(27)	116

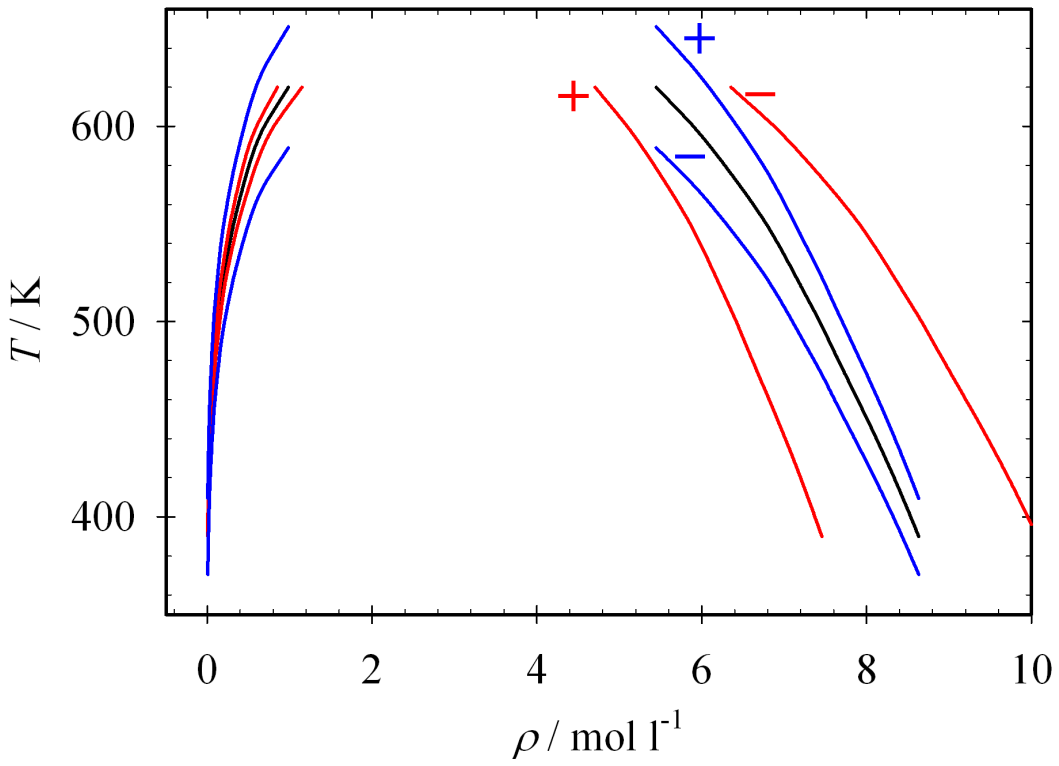

Figure 1: Saturated densities of cyclohexanol: — baseline, — variation of ε_R, — variation of σ_R, + indicates a increase of 5 %, - indicates a decrease of 5 %.

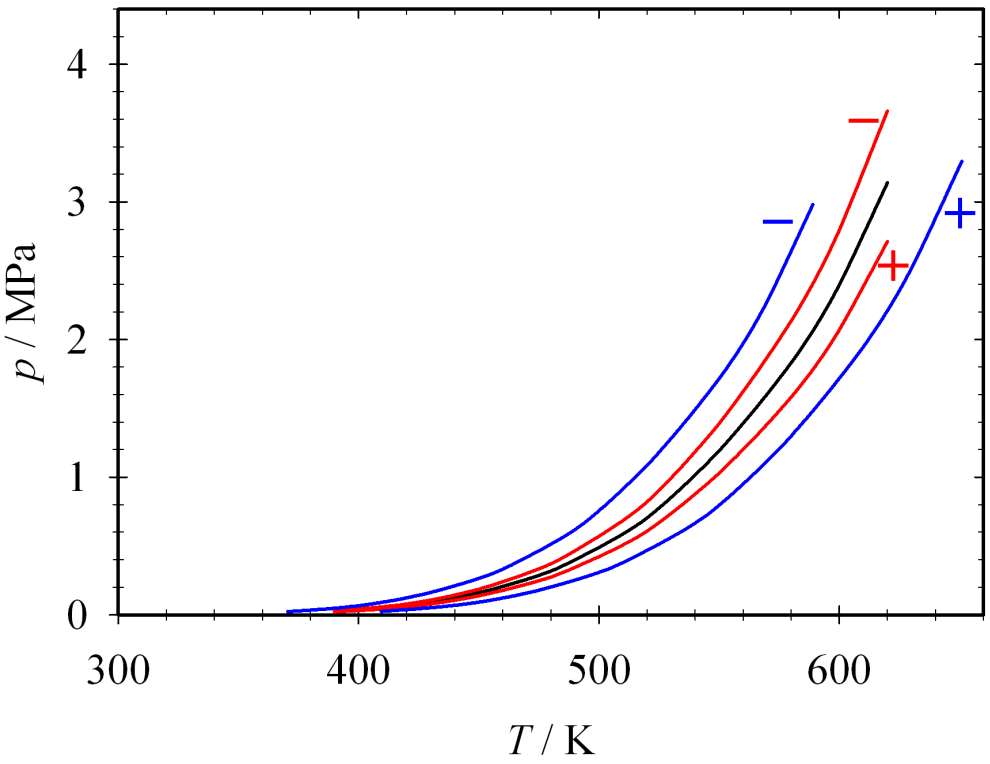

Figure 2: Vapor pressure of cyclohexanol: — baseline, — variation of ε_R, — variation of σ_R, + indicates a increase of 5 %, - indicates a decrease of 5 %.

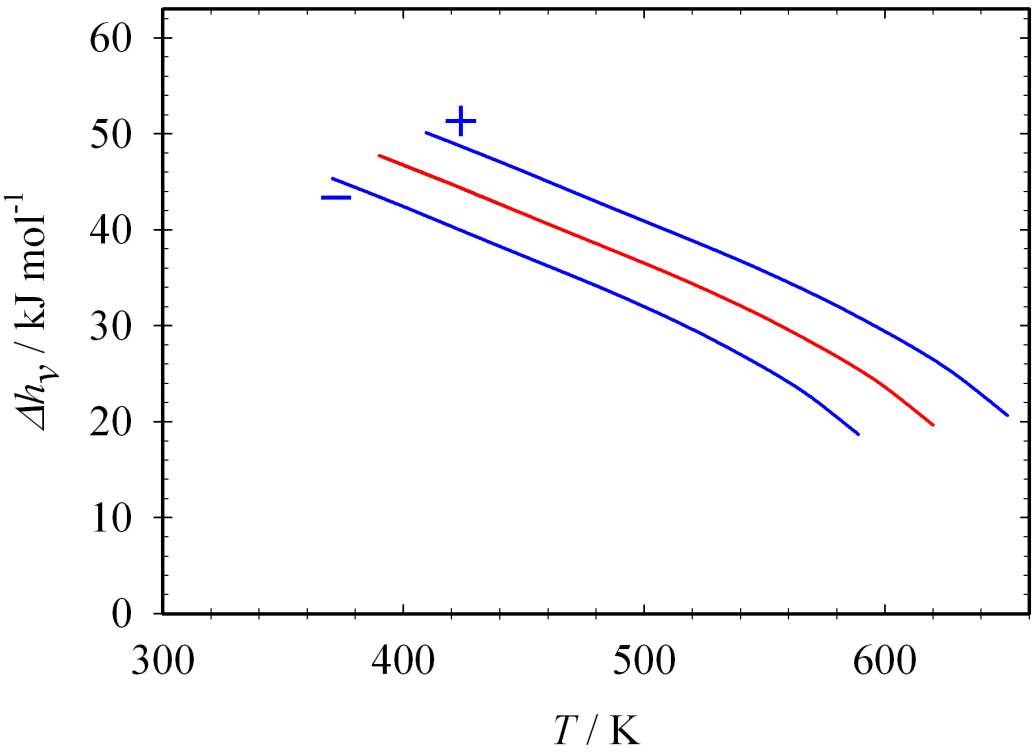

Figure 3: Enthalpy of vaporization of cyclohexanol: — baseline, — variation of ε_R, — variation of σ_R, + indicates a increase of 5 %, - indicates a decrease of 5 %. Note that the red lines coincide with the baseline.

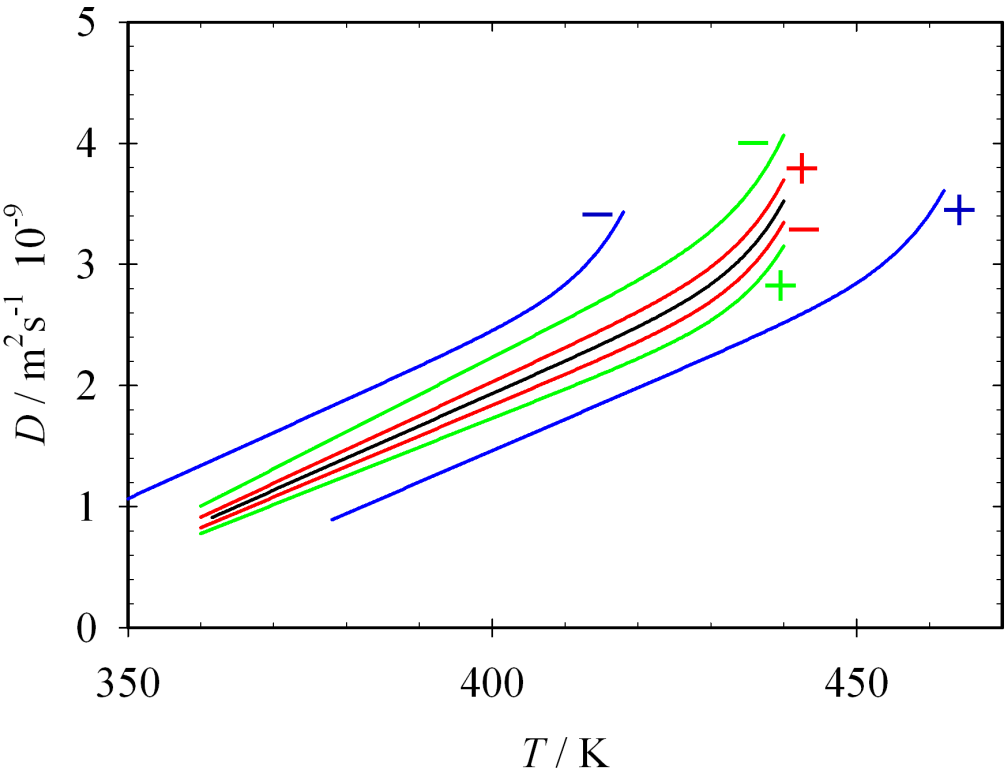

Figure 4: Self-diffusion coefficient of cyclohexanol: — baseline, — variation of ε_R, — variation of σ_R, — variation of m_R, + indicates a increase, - indicates a decrease.

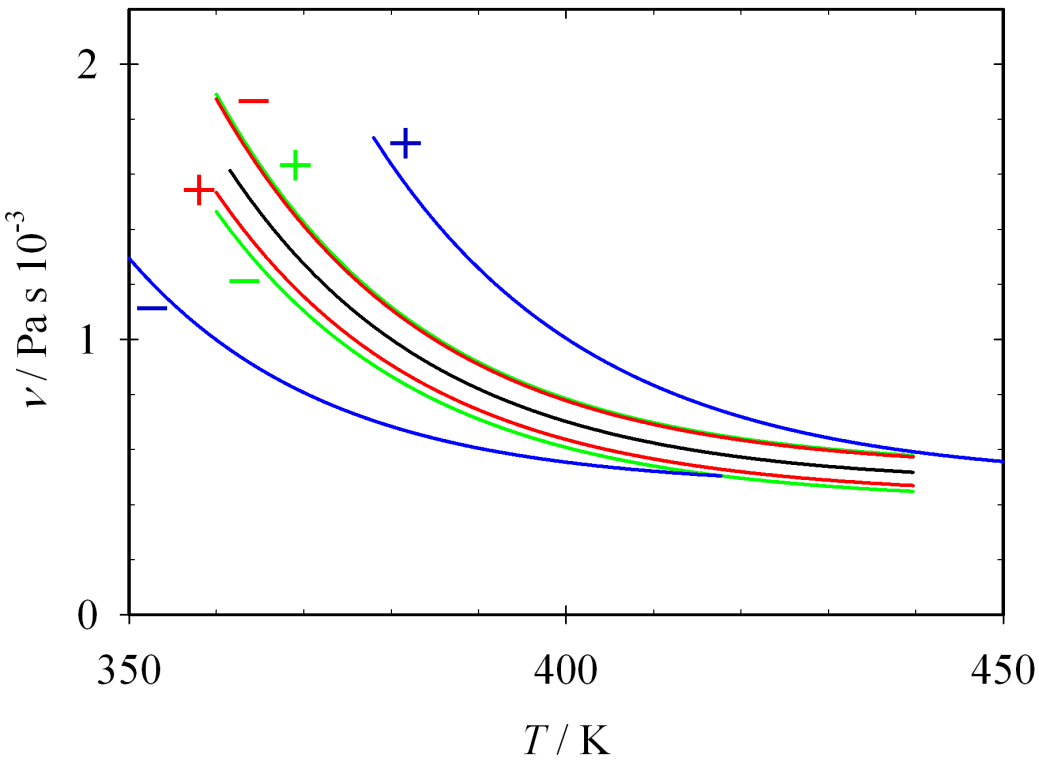

Figure 5: Shear viscosity of cyclohexanol: — baseline, — variation of ε_R, — variation of σ_R, — variation of m_R, + indicates a increase, - indicates a decrease.

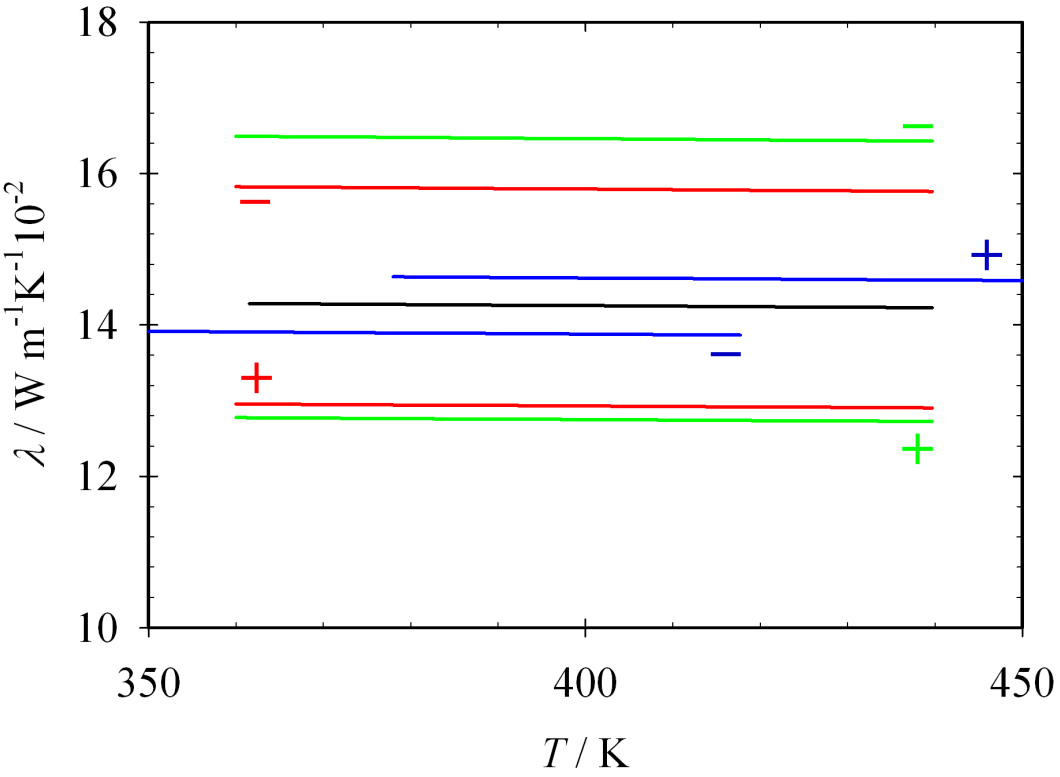

Figure 6: Thermal conductivity of cyclohexanol: — baseline, — variation of ε_R, — variation of σ_R, — variation of m_R, + indicates a increase, - indicates a decrease.

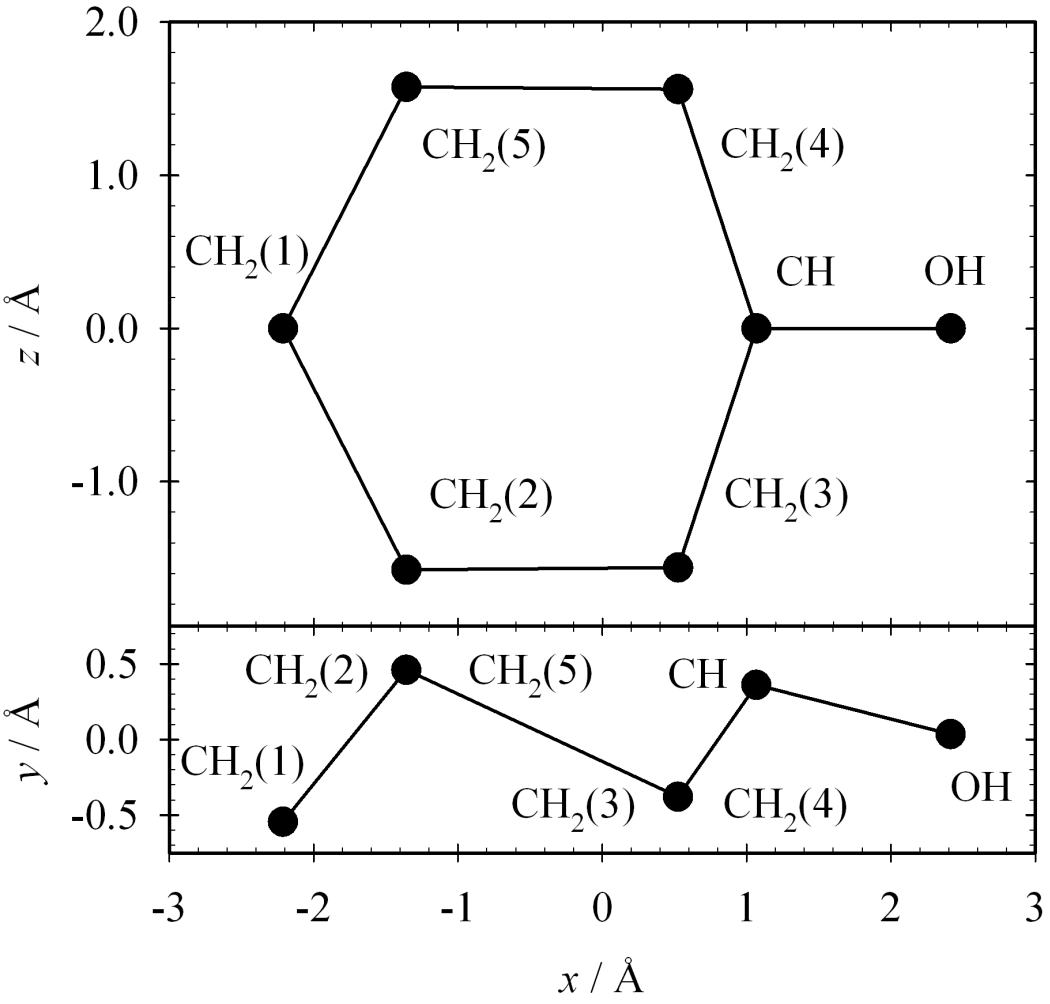

Figure 7: Coordinates of the LJ sites of the present cyclohexanol model.

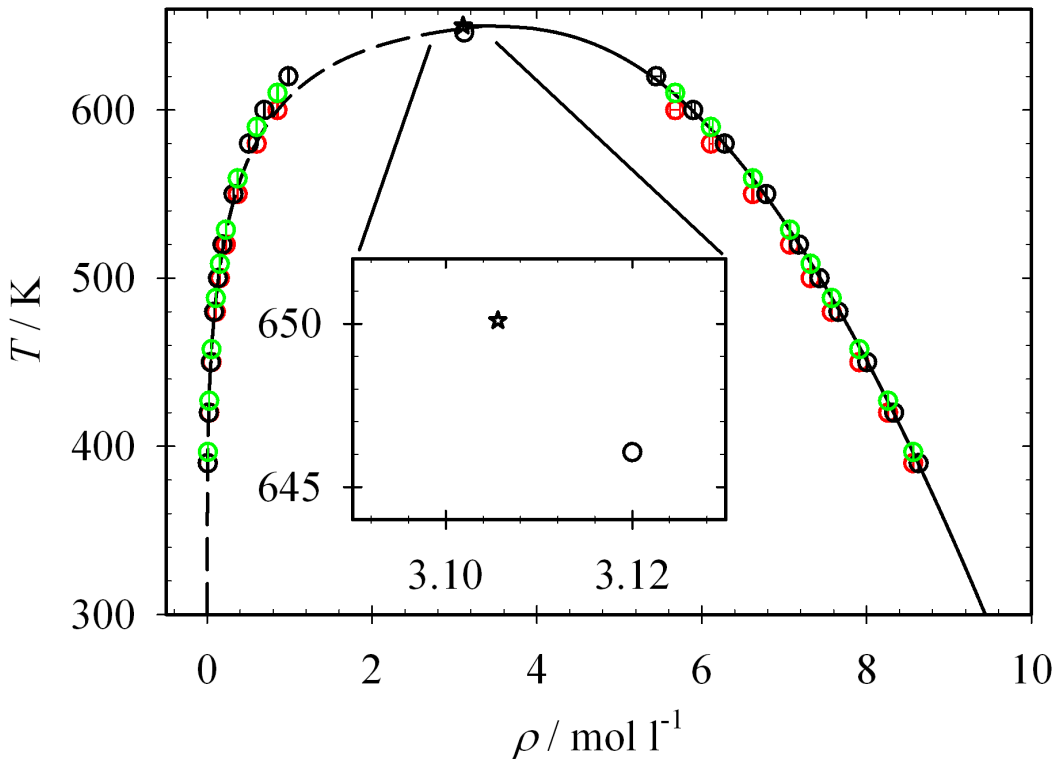

Figure 8: Saturated densities of cyclohexanol: ○ model after first step of optimization, ○ model after reduced unit method, ○ final model, — DIPPR correlation (20), ⋆ experimental critical point (20). Inset: Magnified view on the critical point.

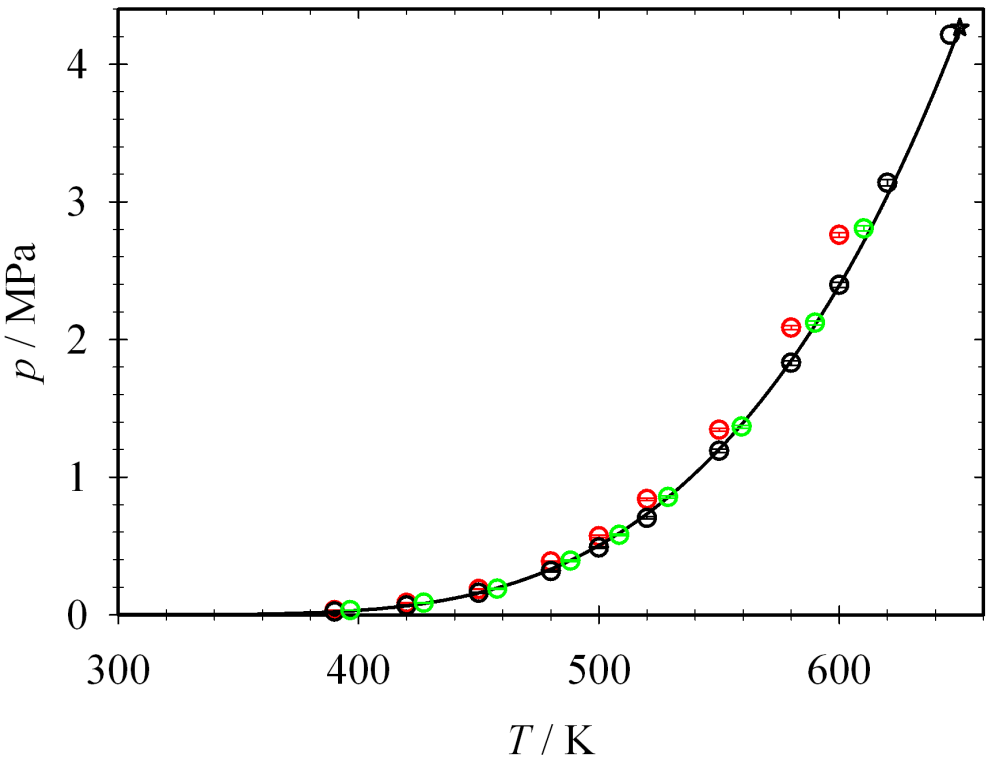

Figure 9: Vapor pressure of cyclohexanol: ○ model after first step of optimization, ○ model after reduced unit method, ○ final model, — DIPPR correlation (20), ⋆ experimental critical point (20).

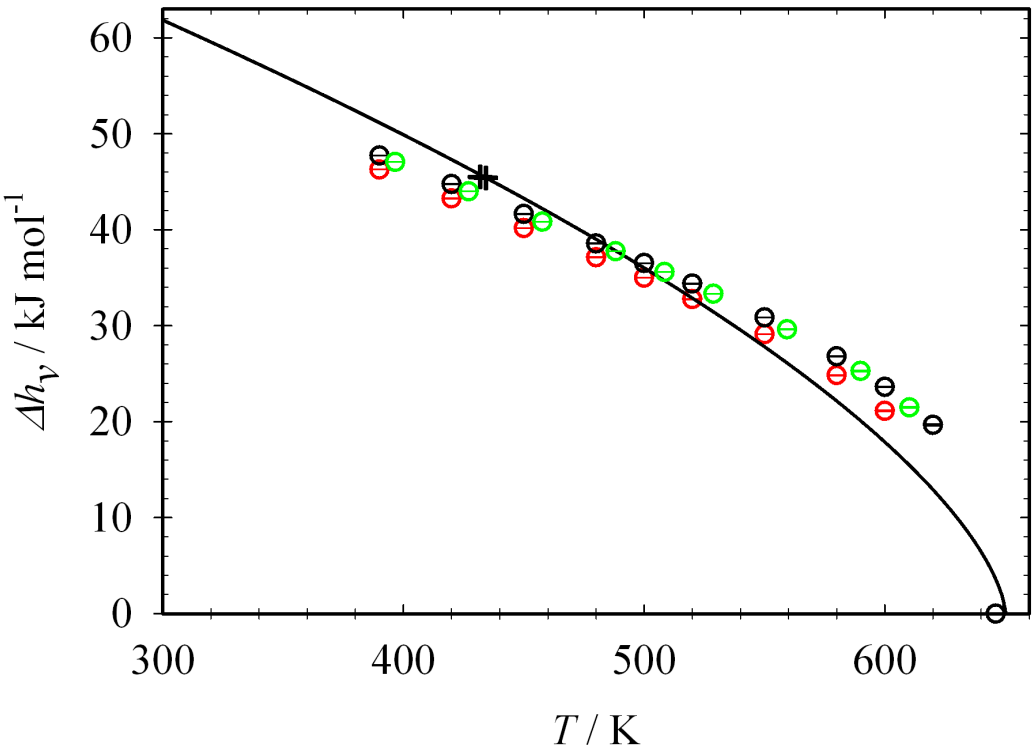

Figure 10: Enthalpy of vaporization of cyclohexanol: ○ model after first step of optimization, ○ model after reduced unit method, ○ final model, — DIPPR correlation (20), + experimental data (23).

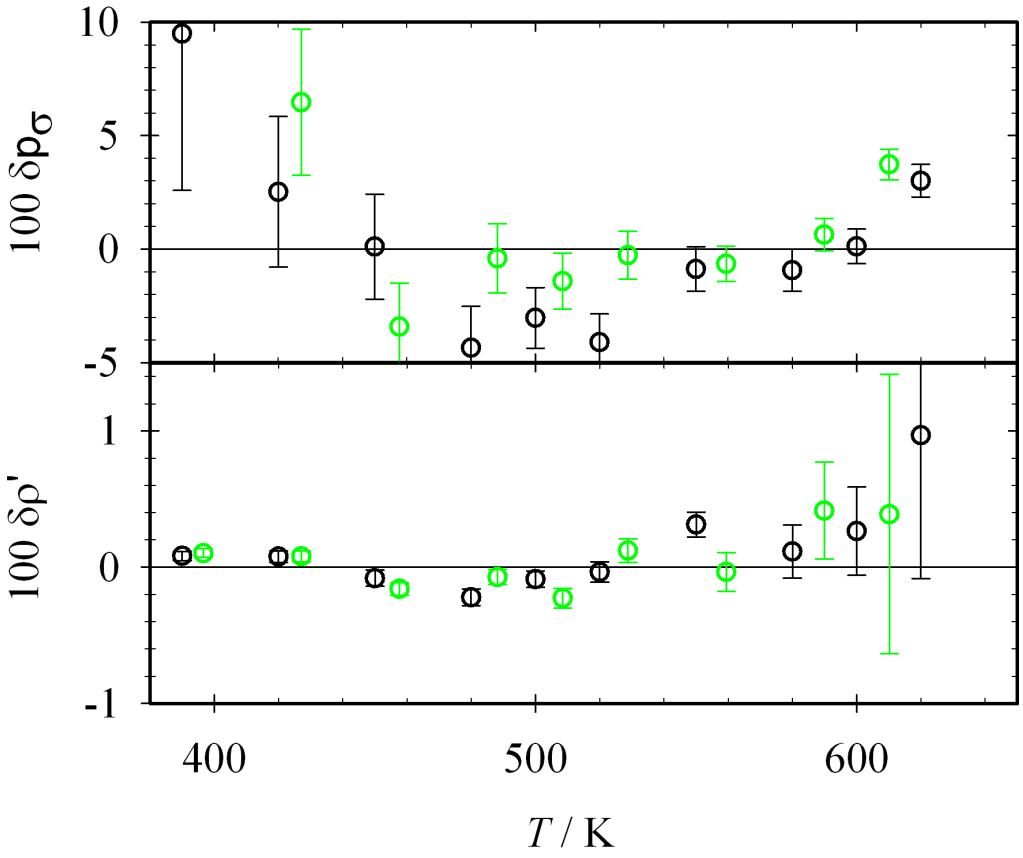

Figure 11: Relative deviations of vapor-liquid equilibrium properties between simulation data and a DIPPR correlation (20) ($\delta z = (z_{\mathrm{sim}} - z_{\mathrm{DIPPR}})/z_{\mathrm{DIPPR}}$): ○ final model, ○ model after reduced unit method. From top to bottom: vapor pressure and saturated liquid density

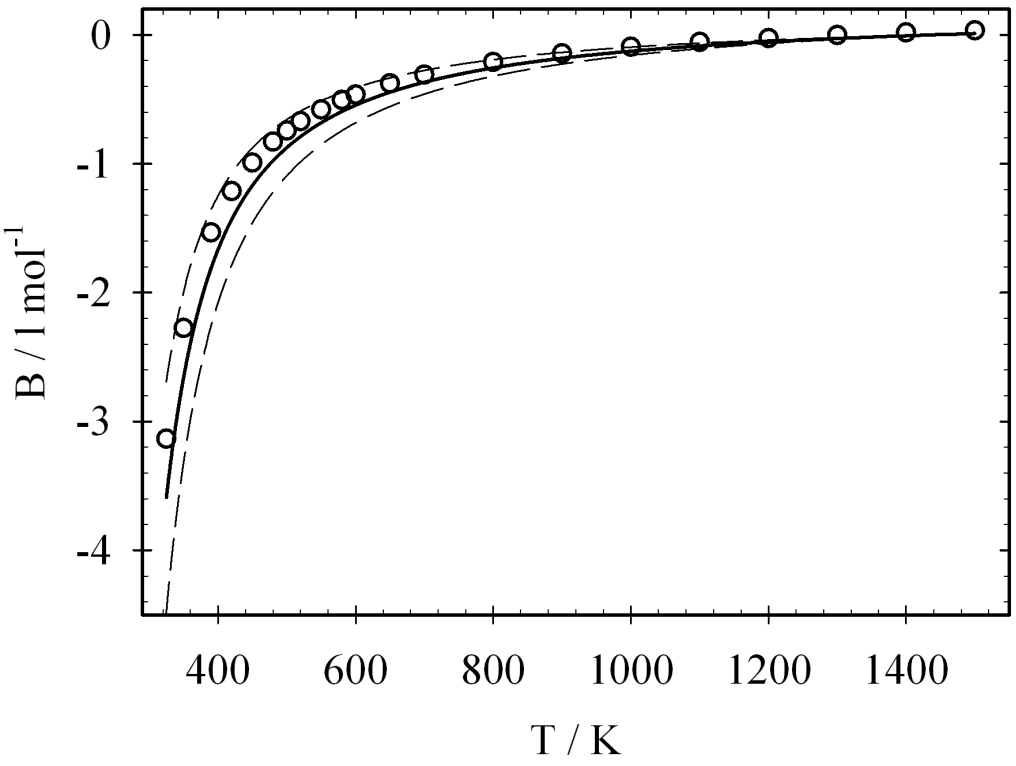

Figure 12: Second virial coefficient of cyclohexanol: ○ final model, — DIPPR correlation (20). The dashed lines indicates the estimated uncertainty of the DIPPR correlation (20).

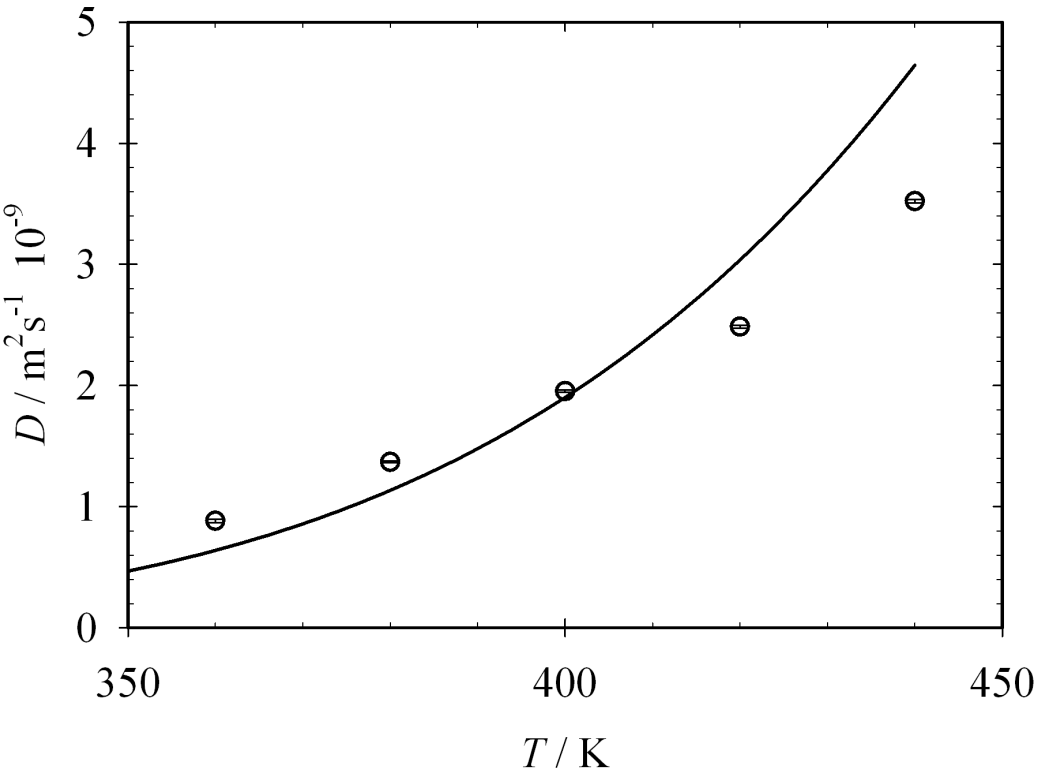

Figure 13: Self-diffusion coefficient of cyclohexanol: ○ final model, — correlation on experimental data (25).

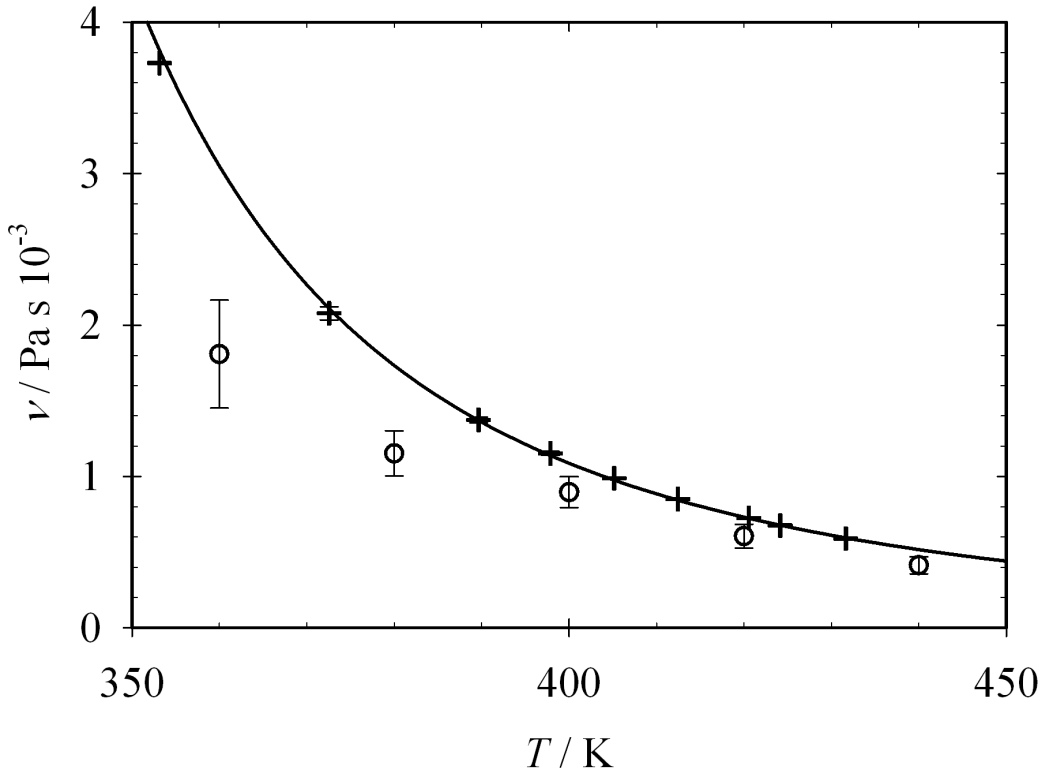

Figure 14: Shear viscosity of cyclohexanol: ○ final model, — DIPPR correlation (20), + experimental data (26).

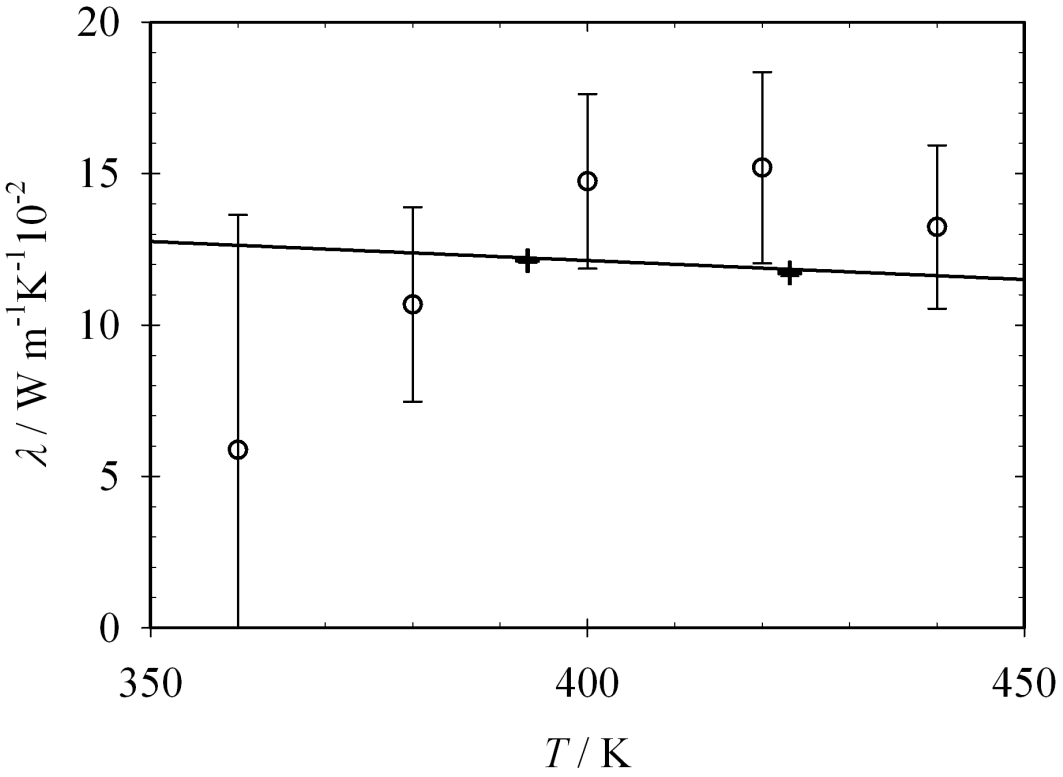

Figure 15: Thermal conductivity of cyclohexanol: ○ final model, — DIPPR correlation (20), + experimental data (27).